



Utrecht University

Master's Thesis in Theoretical Physics

Phase Behaviour of Dumbbell and Barbell Shaped Particles

Supervisors : Prof. Dr. Marjolein Dijkstra & Prof. dr. René van Roij
Author : Tigernach Feehilly

Utrecht University
2021-2022

Abstract

We investigate the phase behaviour of colloidal hard dumbbell and barbell shaped particles. We model dumbbell shaped particles as hard spherocylinders with a length-diameter ratio of L/D which carry spheres of diameter σ at both ends. For the barbell shaped particles, we modify these dumbbells by replacing the spheres with spherocylinders of length L_e and diameter σ . Using Monte Carlo simulations, we map out the phase diagram of these particles for varying aspect ratios of length to diameter (L/D), sphere diameter to rod diameter (σ/D) and barbell end spherocylinders length to rod diameter (L_e/D). As part of our study we investigate the stability of a possible cholesteric phase. Colloids and other achiral particles rarely exhibit a cholesteric phase, thus we take particular interest in investigating the existence of the cholesteric phase in this system. Our results show the destabilisation of the nematic phase, with respect to the isotropic phase, with increases of σ/D . In contrast increases in L/D stabilise the nematic phase. Additionally the spheres and spherocylinders destabilise the smectic phase and crystal phase but allow the formation of a columnar phase. The stability of the smectic phase decreases with L_e/D .

Contents

1	Introduction	2
1.1	Liquid Crystals	2
1.2	Self-Assembly	3
1.3	Dumbbell Shaped particles	3
1.4	Cholesteric Phase and Dumbbells	4
2	Methods	6
2.1	Monte Carlo Simulations	6
2.2	Spatial Hashing	7
2.3	Elongated particles	8
2.4	Linked Lists	8
3	Results	10
3.1	Order parameters	10
3.2	Dumbbells	10
3.3	Cholesteric: Double-twisted columns	13
3.4	Barbells	17
4	Conclusion	21

Chapter 1

Introduction

1.1 Liquid Crystals

As we are taught growing up there are three common phases of matter; solids, liquids, and gasses. Certain systems can exhibit intermediate phases, e.g. liquid crystals, which exist between solid and liquid. Crystal structures have high positional order while liquids have no such order allowing particles to flow freely. Liquid crystals on the other hand have orientational order but no positional order, or only partial positional order. The most common types of liquid crystals are nematic, cholesteric, and smectic phases. The nematic phase exhibits orientational order as the particles align along a common direction but lack positional order, allowing flow. Cholesteric phases, like the nematic phase, have no positional order. Instead particles are aligned along a common direction that rotates through space. The smectic phase has orientational order and positional order in one direction forming layers perpendicular to the orientational order. Finally in a columnar phase as the name suggests the particles are organised into columns and display two-dimensional positional order.

There is much interest in understanding the macroscopic behaviour of these phases from the microscopic details of the constituents and the thermodynamic conditions. Different phases unsurprisingly display differing characteristics, making them useful for different tasks. Nematic phases can be aligned using electric fields and are used in Liquid crystal display (LCD)-screens. The cholesteric phase reflects different wavelengths of light depending on the pitch of the twist.

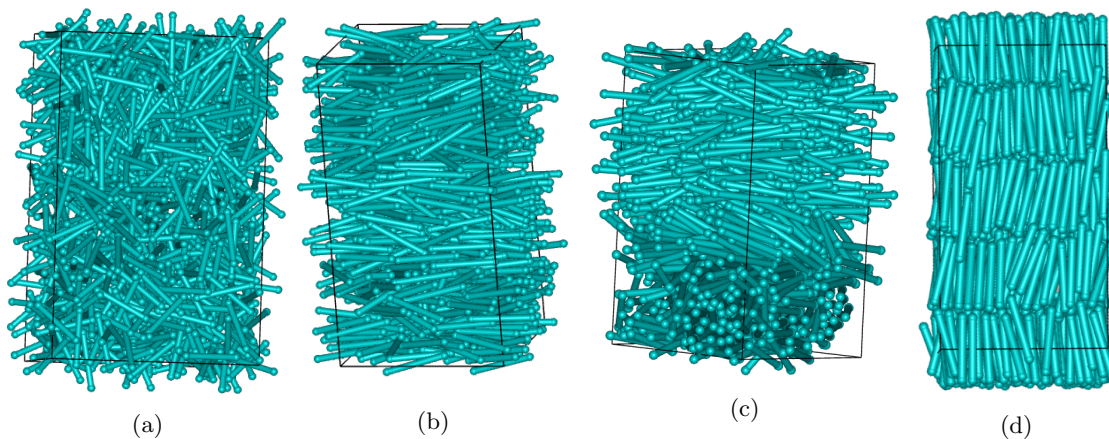


Figure 1.1: Typical configurations of the a) isotropic, b) nematic, c) cholesteric, and d) smectic phase of dumbbell shaped particles.

1.2 Self-Assembly

In this thesis we study the self-assembly of a colloidal suspension of dumbbells. Colloids are insoluble particles with a size in the range of a few nanometers to a few micrometers. Typically, colloids are suspended in a gas or liquid and given their size, collisions with air or liquid particles change the colloids' velocity. With the large number of particles colliding with the colloids from all directions, the colloids are kept in constant random movement called Brownian motion.

Brownian motion allows the colloids to self-assemble into different phases. In this thesis we consider hard particles that cannot overlap, and have no other interactions with each other. Compression causes spontaneous transitions from more disordered phases to ordered phases, i.e. isotropic to nematic. Such a phase transition spontaneously occurs if it results in a lower Helmholtz free energy F of the system,

$$F = U - TS \quad (1.1)$$

where U denotes the internal energy, T the temperature, and S the entropy of the system.

Fixing the temperature and density, the only way to minimise the Helmholtz free energy of a system consisting of hard particles is by increasing the entropy

$$S = k_B \ln \Omega, \quad (1.2)$$

where Ω denotes the number of microstates of the system. A phase transition can occur in a system of hard particles if this results in an increase in entropy.

1.3 Dumbbell Shaped particles

Dumbbell Shaped particles can be synthesised using methods such as those developed by Huang *et al.*[1] amongst others [2, 3]. These particles can be modelled as a system of hard particles. Therefore simulations can inform experimental investigation into the phase behaviour of the system, saving time and resources. In this thesis we investigate the phase behaviour of dumbbell shaped particles, that consist of a cylinder with length L and diameter D and two spheres centered on the circular faces of the cylinder with diameter σ as illustrated in Fig 1.2a).

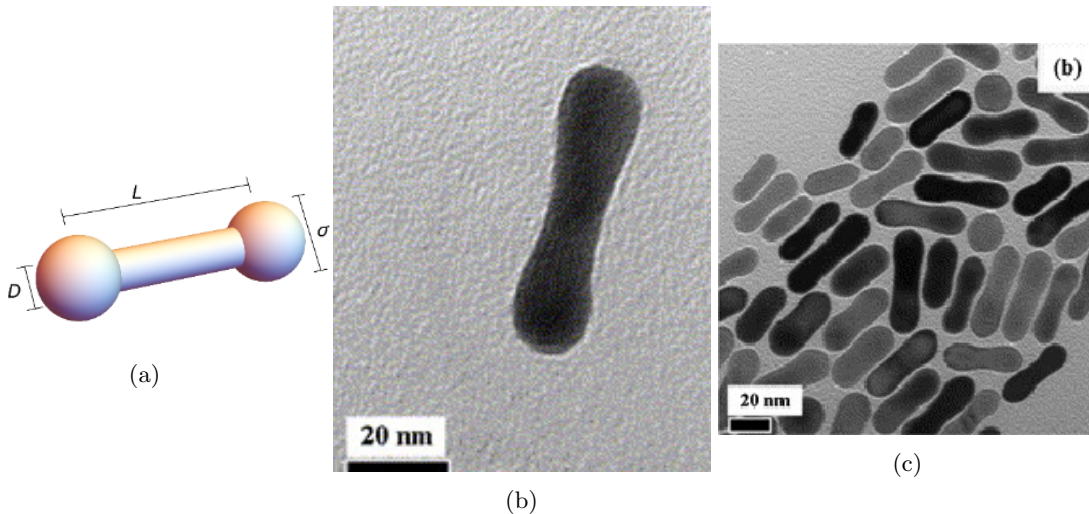


Figure 1.2: a) Schematic picture of the dumbbell shaped particles used in our simulations, where L is the length of the cylinder, D the diameter of the cylinder, and σ the diameter of the end spheres. b) and c) show examples of an experimental system of colloidal dumbbells taken from Ref. [1].

Modelling the Dumbbells

We model the dumbbells as hard particles shown in Fig. 1.2a. The overlap of particles is not allowed. The volume of individual dumbbells is given by the volume of the cylinder and the 2

partial spheres on the ends. The volume occupied by the spheres and the cylinder is given by

$$V = 16\pi h(3\frac{D^2}{2} + h^2). \quad (1.3)$$

This gives the sphere volume as $V_S = \frac{4}{3}\pi\frac{\sigma^3}{2} - V$ and the cylinder volume as $V_C = \pi(L - 2(\frac{\sigma}{2} - h))(\frac{D}{2})^2$. The total volume is then

$$V_T = 2V_S + V_C. \quad (1.4)$$

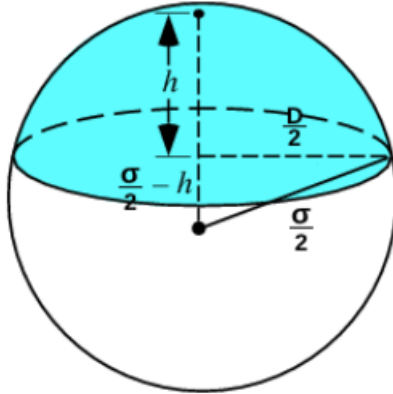


Figure 1.3: In blue the sphere section "inside" the central cylinder.[4]

1.4 Cholesteric Phase and Dumbbells

A cholesteric phase is characterised by a local orientational order but no positional order, it also has a twist to the orientation along an axis as show in Fig. 1.4.

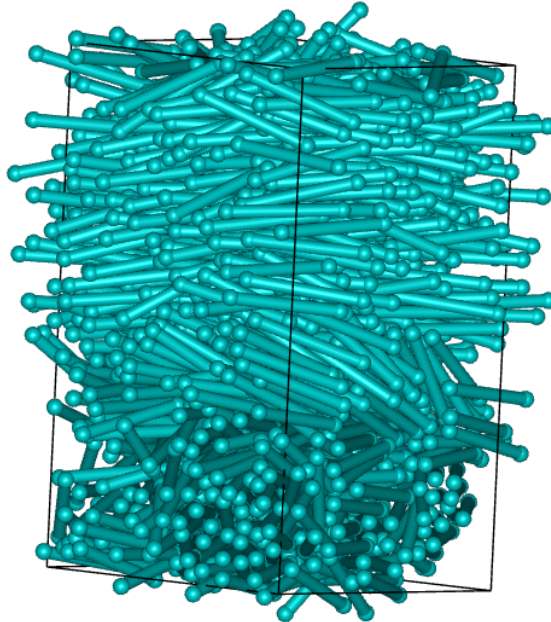


Figure 1.4: Example of twisting orientation in the cholesteric phase for dumbbell particles.

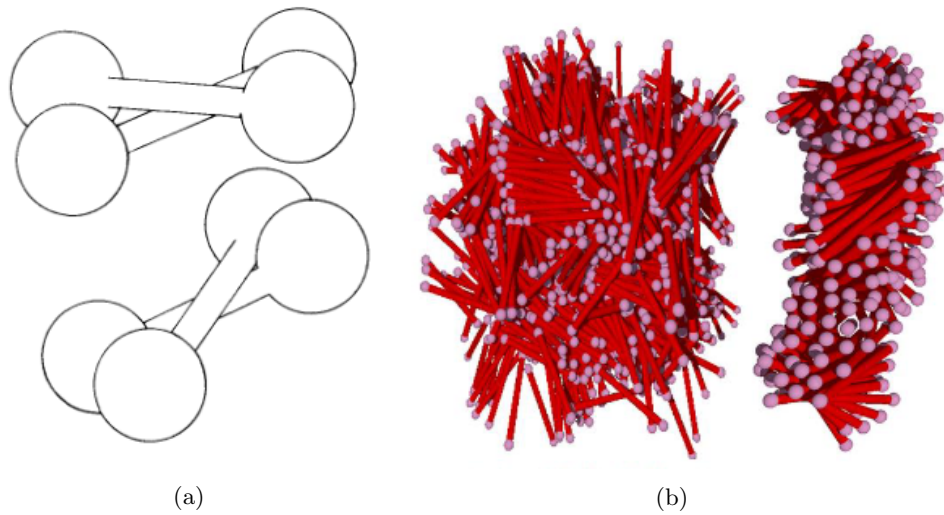


Figure 1.5: a) De Gennes depiction of the twist of dumbbell shaped particles. Taken from [6]. b) Example of the double twisted column from [3].

Typically, cholesteric phases form when chiral particles are dissolved into a nematic phase, causing the nematic system to become twisted [5], or in systems of pure cholesterol esters. Formation of cholesteric phases from achiral systems or molecules such as dumbbells is of great interest. De Gennes originally predicted the cholesteric phase of dumbbells in his book [6] as early as 1993. In Fig. 1.5a De Gennes depicts how the convex shape and the rotated orientation allow for tighter packing of particles.

In this work we will investigate the existence of the predicted cholesteric phase of dumbbells and test whether it is stable not just metastable. Previous works by Yang *et al.*[3] have found densities at which chiral features exist. However, Yang found a double-twisted chiral columnar phase shown in Fig. 1.5b. This double-twisted phase shows a localised correlation of direction of particles along a twisting nematic director but contrasts the cholesteric mesophase in which all particles within a plane perpendicular to the twist orientate themselves along the same direction shown in Fig. 1.4.

Chapter 2

Methods

2.1 Monte Carlo Simulations

We employ Metropolis Monte Carlo simulations to simulate the phase behaviour of dumbbell and barbell shaped particles. In a Monte Carlo simulation we generate a set of configurations of the system from a probability distribution. This set is typically a good representation of the system.

Looking at the canonical ensemble, i.e. N , the number of particles, V , the volume of the system, T , the temperature of the system, are all constant. To do this we describe the system using the Hamiltonian:

$$H(\mathbf{r}^N, \mathbf{p}^N) = \sum_{n=1}^N \frac{\mathbf{p}_n^2}{2m} + U(\mathbf{r}^N) \quad (2.1)$$

where \mathbf{p}_i is the momentum of the i^{th} particle, m the mass and $U(\mathbf{r}^N)$ the potential energy of the system, \mathbf{r}^N the positions of all N particles.

As dumbbells are not spherically symmetric the orientation of particles is important. The orientation of a particle is given by a unit vector in \mathbb{R}^3 . This vector points from the centre of mass to one end of the particle. With all this the potential between two particles becomes:

$$U(\mathbf{r}_i, \mathbf{w}_i, \mathbf{r}_j, \mathbf{w}_j) = \begin{cases} \infty & \text{if the particles overlap} \\ 0 & \text{otherwise} \end{cases} \quad (2.2)$$

therefore only configurations without overlaps are accepted.

Another more complete description of the system is given by the partition function:

$$Z(N, V, T) = \frac{1}{N! \lambda^{3N}} \int d\mathbf{r}^N \exp(-\beta U(\mathbf{r}^N)) \quad (2.3)$$

where λ denotes the thermal wavelength, $\beta = 1/k_B T$, and k_B Boltzmann's constant.

From this we can derive the average value for an observable O , such as the pressure of the system or an order parameter

$$\langle O \rangle = \frac{\int d\mathbf{r}^N O(\mathbf{r}^N) \exp(-\beta U(\mathbf{r}^N))}{\int d\mathbf{r}^N \exp(-\beta U(\mathbf{r}^N))}. \quad (2.4)$$

Calculating this exactly requires calculating the numerator and denominator for all possible configurations of the particles. If O and U are given by an equations that allow us to perform the integrals analytically this can be calculated exactly. However, more often than not this is impossible. Instead of integrating over all \mathbf{r}^N we generate samples $\mathbf{r}_1^N, \mathbf{r}_2^N, \mathbf{r}_3^N, \dots, \mathbf{r}_m^N$, calculating O as:

$$\langle O \rangle = \frac{1}{m} \frac{\sum_{i=1}^m O(\mathbf{r}_i^N) \exp(-\beta U(\mathbf{r}_i^N))}{\sum_{i=1}^m \exp(-\beta U(\mathbf{r}_i^N))} \quad (2.5)$$

Generating $\mathbf{r}_1^N, \mathbf{r}_2^N, \mathbf{r}_3^N, \dots, \mathbf{r}_m^N$ begins with an initial configuration \mathbf{r}_{init}^N . Making small random changes to the positions of particles to generate a new configuration \mathbf{r}_{trial}^N , which is accepted with probability:

$$acc(\mathbf{r}_{init}^N \rightarrow \mathbf{r}_{trial}^N) = \min(1, \exp(-\beta U(\mathbf{r}_{trial}^N) - \beta U(\mathbf{r}_{init}^N))) \quad (2.6)$$

If \mathbf{r}_{trial}^N is accepted it acts as \mathbf{r}_{init}^N and we generate another trial configuration from small random changes of \mathbf{r}_{trial}^N . Otherwise, we generate another trial from \mathbf{r}_{init}^N . This process is repeated until the system reaches equilibrium and enough configurations \mathbf{r}_i^N are generated to calculate the average observable.

Described above simulations used constant N , V , and T . However, NPT simulations have their advantages. With NPT the pressure P is constant rather than volume V , changing V to keep P constant. Similarly to changing the positions described before, trial changes to volume V_{trial} are attempted and positions \mathbf{r}_{init}^N scaled with the change in volume. Volume trial changes are accepted with probability:

$$acc(V_{init} \rightarrow V_{trial}) = \min(1, (\frac{V_{trial}}{V_{init}})^N \exp(-\beta P(V_{trial} - V_{init}) - \beta U(\mathbf{r}_{trial}^N) - \beta U(\mathbf{r}_{init}^N))). \quad (2.7)$$

2.2 Spatial Hashing

In simulations there is always limited computing power available. Even with powerful machines efficient use of computational power is required. In simulations of hard particles checking overlaps is a prime place for improvements in efficiency. The most basic algorithm for checking overlaps calculates the distances between every pair of particles in the system. Reducing the number of pairs needed would greatly speed up the process.

With dumbbell shaped particles 9 checks for overlaps are needed to make sure that no overlaps have occurred, four between the two end spheres, four between end spheres of one particle and the centre cylinder of the other, and one between the cylinders of the particles. We use the method described in [7] to calculate the possible cylinder-cylinder and sphere-cylinder overlaps.

We wish to avoid checking overlaps between particles that have no chance of overlapping. For example, the distance between centres is quick to calculate and can rule out overlaps for the majority of particles in the simulation. Therefore, instead of checking all nine possible overlaps for all particles, only those with a centre distance less than or equal to the total length of the particles (length of cylinder plus twice the diameter of the sphere) need to be checked. This approach, though helpful, is open to improvement.

Instead of calculating centre distances to rule out overlaps each time the system changes, a list keeping record of the possible overlaps would be more efficient. To do this we implement spatial hashing, beginning by dividing the simulation box into cells. For each cell a list is created storing the *id* of all particles in that cell.

When possible collisions are calculated only particles in the same or neighbouring cells can have overlaps and all other particles can be safely ignored. Keeping lists allows for all relevant particles for an overlap to be found by retrieving values in memory instead calculating distances for all particle pairs, speeding up the simulation.

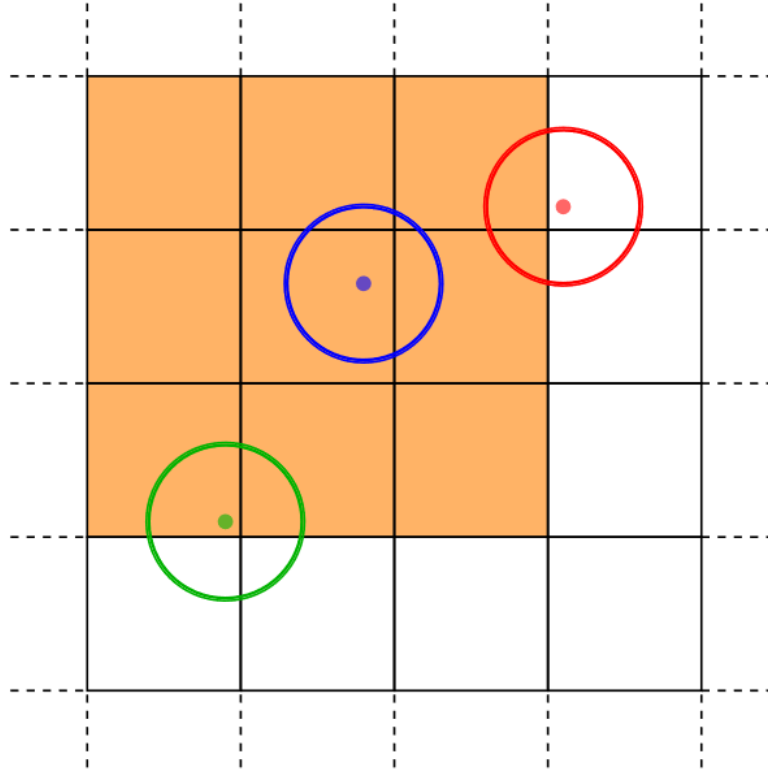


Figure 2.1: Simulation divided into cells. A list is created for each cell. Here we see the blue particle is not overlapping with either red or green. However, the the blue and green particles if moved in their cells can overlap without leaving the cell. However red and blue cannot overlap at all without moving to other cells.

Looking up potentially overlapping particles is now possible and the number of checks needed to find overlaps is reduced. However, one important note, dumbbell shaped particles occupy multiple cells as described in the next section and do not stretch. Thus when the system changes volume the lists are refilled each time. This is effectively spatial hashing which can improve performance depending on the problem [8, 9] and has been shown to aid this problem.[4]

2.3 Elongated particles

Elongated particles cross multiple cells and this needs to be shown in the lists storing the particles in each cell. To efficiently calculate the cells occupied by a particular particle, the particle is completely bounded by spheres. The spheres have diameter equal to the length of the cells, and are placed along the particle. They are placed such that the intersection of any two sphere surfaces form a circle, with a radius greater than the diameter of the central cylinder. The occupied cells are then any cell containing the centres of the spheres.

The spheres must bound the particle, thus they must be as big if not larger in diameter as the diameter of the cylinder or the end spheres and overlap, so that no part of the particle exists outside a bounding sphere.

2.4 Linked Lists

Each cell needs to keep track of the particles in it. As each list may be of different lengths and we do not know the lengths beforehand, we make use of linked lists. Linked lists are memory efficient and have variable length. The elements of a linked list are nodes containing the *id* for a particle

and a pointer to the location of the next node in memory in the list. This list of nodes terminates with a node with $id = -1$ and the pointer pointing to $NULL$. There also exists a list of head nodes, these head nodes point to a start the start of a particular linked list. Fetching the particles of interest then involves going to the head node of a cell that could contain an overlap. From the pointer of the head node going to the start of the linked list. The first id number is fetched and the pointer tells us where the next node is stored in memory. The list is then worked through collecting the ids and moving on to the next pointer until a node with and id of -1 is reached. The collected ids are then checked for collision.

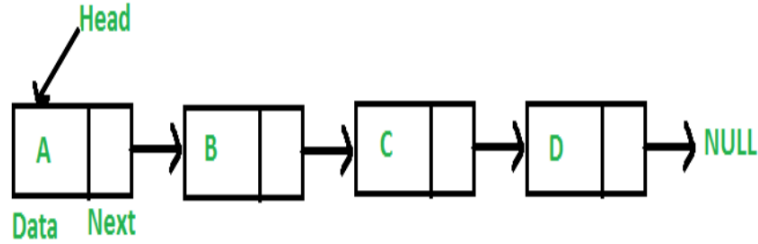


Figure 2.2: The structure of a linked list. A head node points to a segment of memory that stores a data value and a pointer to the next block of memory and so on until the end of the list is reached which points to null.

Using a 3D array of pointers, one for each cell pointing to a unique head node for each list, efficient calls to the correct lists can be done. This method of listing does not offer all the functions of an array, but it uses less memory than creating an array for each cell and the complete functionality of an array is not needed. For example, when collision checks are to be carried out, all particles in a cell of interest are needed, never a subset. Thus all particles in a relevant cell are visited and we do not need to know if it is the n^{th} or the $(n + 1)^{th}$ element.

Chapter 3

Results

3.1 Order parameters

To classify the phases of a system order parameters are needed. These are measurements of the system that are zero in one phase and non-zero in another. To classify the nematic phase, defined as having orientational order but no positional order, we need a measurement that is non-zero when alignment of the particles occurs and zero otherwise. This is called the global nematic order parameter S . S is defined as the maximum eigenvalue of the matrix

$$Q_{\alpha\beta} = \frac{1}{N} \sum_{i=1}^N \left[\frac{3}{2} \mathbf{u}_{i\alpha} \mathbf{u}_{i\beta} - \frac{\delta_{\alpha\beta}}{2} \right], \quad (3.1)$$

where N is the number of particles in the configuration, $\mathbf{u}_{i\alpha}$ is the α^{th} component of the vector describing the orientation of the i^{th} particle, and $\delta_{\alpha\beta}$ is the usual Kronecker delta. The value of S ranges from 0 for random orientations to 1 for completely aligned.

The second order parameter of interest is the smectic order parameter. This will be non-zero when there is layering along the direction of the nematic director, and is given by

$$\tau = \max_l \left| \sum_{j=1}^N e^{2\pi \mathbf{r}_j \cdot \mathbf{n} / l} \right|, \quad (3.2)$$

\mathbf{n} is the nematic director, the eigenvector that goes with S , \mathbf{r}_j the position of the j^{th} particle and l the distance between layers found when maximising τ with respect to l in (3.2).

3.2 Dumbbells

We model the dumbbells as described in section 1.3. The stability of a smectic phase of elongated rod-like particles such as spherocylinders has been shown to depend on the number of smectic layers in the simulation box [10]. The work by Dijkstra *et al.* found that due to finite size effects, smectic phases lack stability in small systems of spherocylinders. They also found that for spherocylinders with values of $L/D \leq 10$, 6 smectic layers allowed stable smectic configurations. In this work, to take advantage of this information, N the total number of particles used in a simulation have a total volume of six times twice L_{Total} the total length of the particle squared.

$$N = \frac{6(2L_{Total})^2}{V}, \quad (3.3)$$

where V is the volume of the particle. This, along with not allowing a side length of the simulation box to be less than 2 times L_{Total} , ensures that particles are never self-interacting due to periodic boundary conditions and there will be sufficient volume to stably form at least 6 smectic layers.

We first perform simulations of hard dumbbell shaped particles with $L/D = 7, 9$ and σ/D in the range $[1, 1.5]$, to check against the work by Gabrielse [4]. For both values of L/D an isotropic, nematic, smectic and columnar phase were found for dumbbell shaped particles. Fig. 3.1 shows the order parameters S and τ for systems of hard dumbbell shaped particles with $L/D = 7$ and $\sigma/D = 1, 1.1, 1.2, 1.4$. Isotropic phases appear at low packing fractions, η , where nematic and smectic order parameters are low for all values of σ/D . For $\sigma/D \leq 1.1$ steep increases in the nematic and smectic order parameters identify the isotropic-nematic and nematic-smectic transitions, respectively. The smectic-crystal transition is shown by the small jump in packing fraction seen for $\sigma/D = 1$. The smectic-columnar transition can be identified by the strong fall of the smectic order parameter with the nematic order parameter remaining high. For the higher values of $\sigma/D > 1.2$ the smectic phase is not present and a nematic-columnar transition occurs with large jumps in the packing fraction and S . Investigation of configurations shown in Fig. 3.2 match with these findings and the work by Gabrielse.

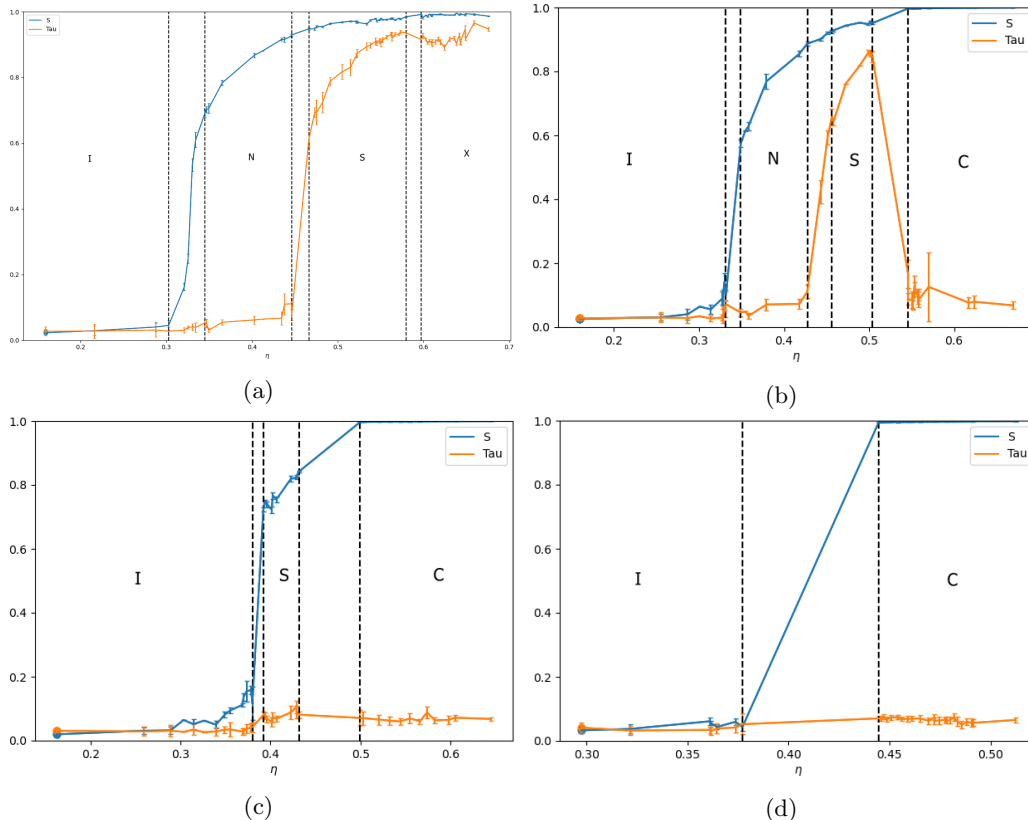


Figure 3.1: Nematic and smectic order parameters plotted against the packing fraction for a system of hard dumbbell shaped particles with $L/D = 7$ and $\sigma/D = 1, 1.1, 1.2, 1.4$, respectively. Points are joined by lines for guidance. Vertical dashed lines show the phase boundaries between the isotropic (I), nematic (N), smectic (S) and crystal/columnar (X/C) phases.

Extending L/D to 9, 13, 15, the results of $L/D = 9$ match previous work and the phase diagrams, Fig. 3.4, show the dependence of the phase transitions on σ/D . The increase of σ/D destabilises the nematic phase with respect to the isotropic phase, the gain in free volume from an increase in directional order being reduced. This effect is dampened with an increase in L/D with the nematic phase persisting to higher values of σ/D , up to $\sigma/D = 1.4$ for $L/D = 9$ and $\sigma > 1.5$ for both $L/D = 13$ and 15.

Focusing on the smectic phase again it is destabilised with increasing σ/D . However, unlike the nematic phase this stability does not return with the increase in L/D disappearing for all values of L/D at $\sigma/D = 1.2$. Within the layers of the smectic phase particles are directionally orientated as well, aligning the spheres along the outside of these layers, thus creating more space between

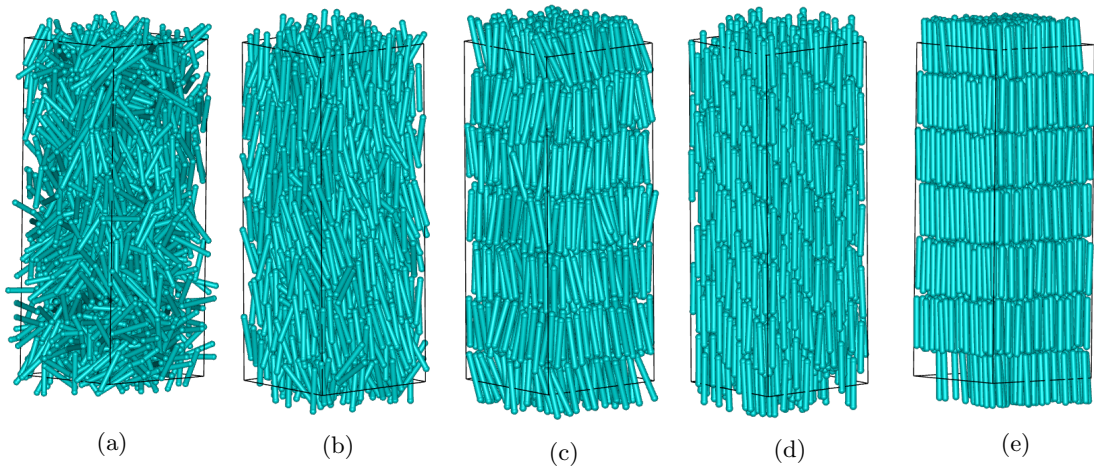


Figure 3.2: a-d) Typical configurations of hard dumbbell shaped particles with a length-to-diameter ratio $L/D = 7$ and $\sigma/D = 1.1$ in the four phases a) isotropic, b) nematic, c) smectic and d) columnar. e) Typical example of crystal phase formed by hard spherocylinders with $L/D = 7$.

particles. The increased space then destabilises the smectic phase.

We did not find a stable cholesteric phase. However, it has been speculated that a cholesteric phase may exist at a density higher than that of the nematic phase, but lower than that of a positionally ordered phase like the smectic, columnar, or crystal phase. We investigate the possible formation of a cholesteric phase later in section 3.3.

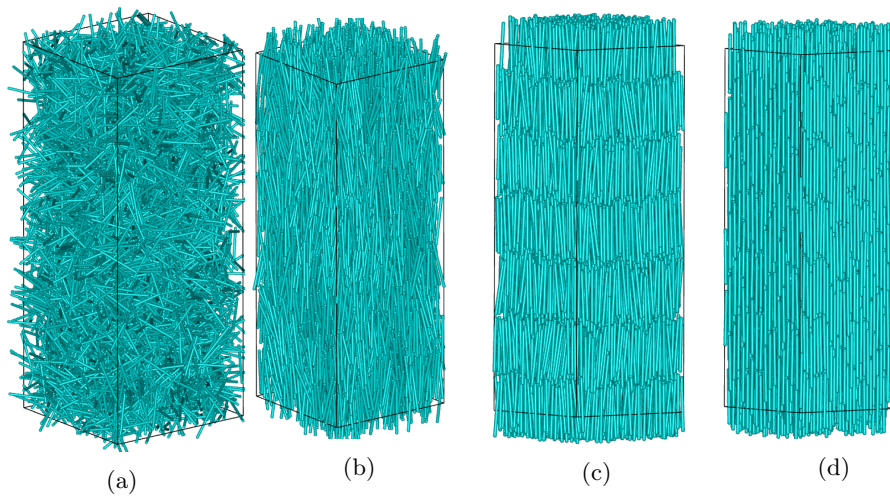


Figure 3.3: Typical configurations of hard dumbbell shaped particles with a length-to-diameter ratio $L/D = 15$ and $\sigma/D = 1.1$ in the four phases a) isotropic, b) nematic, c) smectic and d) columnar.

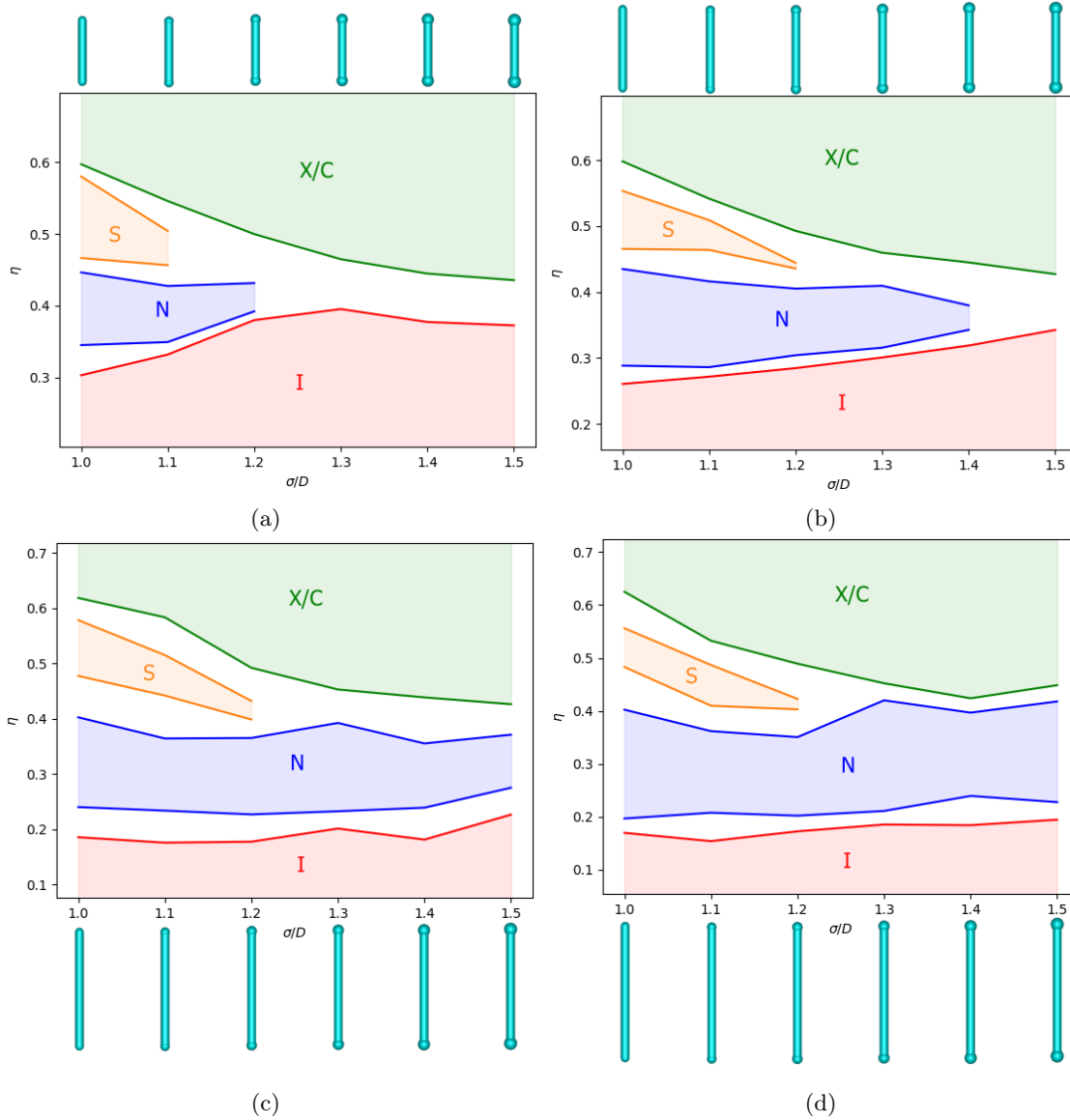


Figure 3.4: Phase diagram of hard dumbbell shaped particles in the packing fraction η -sphere diameter to rod diameter σ/D representation with a length to diameter ratio of a) $L/D = 7$, b) $L/D = 9$, c) $L/D = 13$ and d) $L/D = 15$. Solid lines denote the limits of the isotropic (I), nematic (N), smectic (S) and crystal/columnar phase (X/C).

3.3 Cholesteric: Double-twisted columns

A study published by Yang *et al.* [3] investigated the phase transition of dumbbell shaped particles. They found a phase they describe as a double-twisted column phase. Within a column particles pack together and neighbouring particles form a hexagonal shape with slightly off set directions, as hypothesised by De Gennes. The column itself is also twisted hence the term double-twisted column. As mentioned before in section 1.4, this is not the usual cholesteric phase that we see with chiral particles. In simulations with systems consisting of $N = 1000$ particles the stability of the smectic phase was suppressed by finite size effects, however this double-twisted state appears when compressing the system. Beginning in the isotropic phase and compressing slowly caused the system to enter a nematic phase and then a columnar phase. Compressing rapidly resulted in the formation of this double-twisted columnar phase. This double twisted phase does not appear when expanding from a crystal or columnar phase.

Due to the symmetry of the particles there is no preference for one direction over another in the twist of the column, leading to a racemic mixture of right- and left-handed chiral columns.

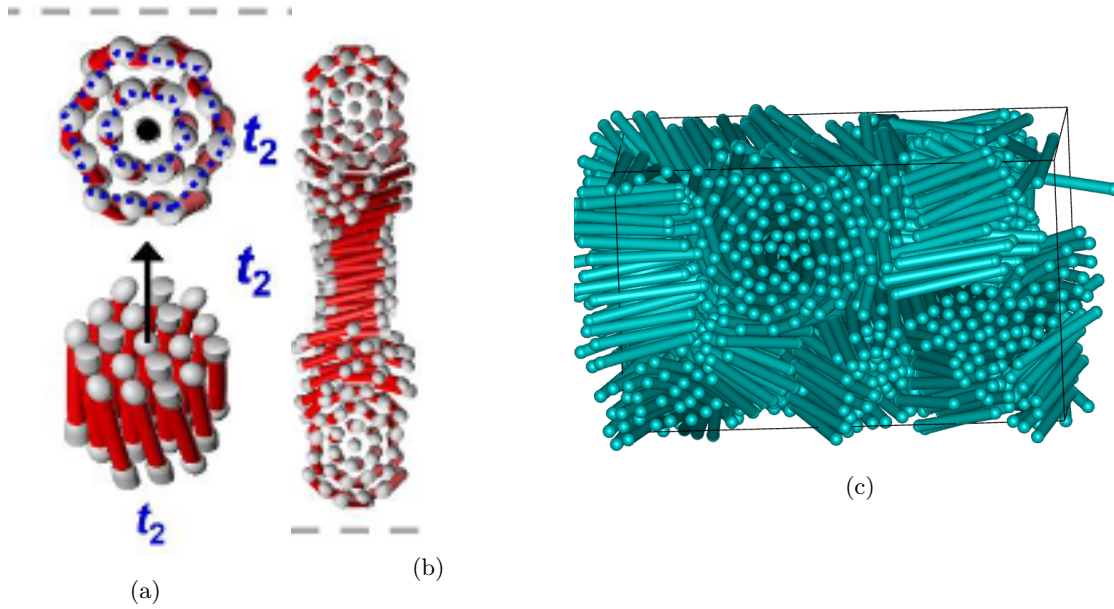


Figure 3.5: a,b) visualisations of local chiral order in an experimental system of dumbbell shaped particles taken from [3]. c) Typical configuration of local chiral order in a system of hard dumbbell shaped particles with $L/D = 9$ and $\sigma/D = 1.1$ as obtained from simulations, showing a racemic mixture of right- and left- handed chiral columns.

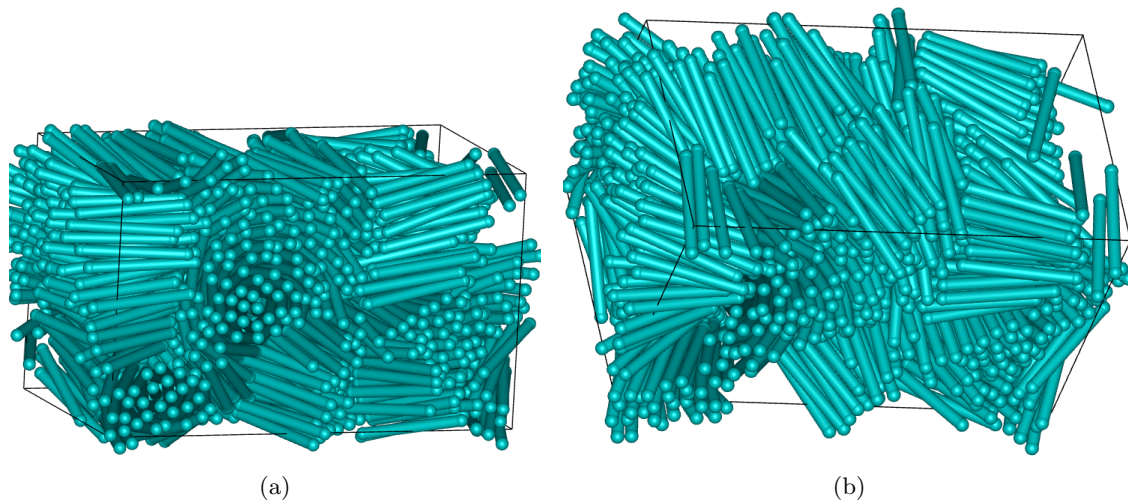


Figure 3.6: The same configuration as in 3.5c but from different viewing angles. Figs. 3.5c and a) show a double twisted column in the top middle. b) shows that the system is different from a cholesteric pure as it only exhibits finite-size domains with local chiral order.

To check that this is not a finite-size effect we looked at larger simulations for $L/D = 9$ with $N > 2000$. We found that these double-twisted columns persisted. In Fig. 3.7, we find that the order parameters S and τ as a function of packing fraction η are very different from those found in section 3.2. With a rapid compression from the isotropic phase the system fails to transition to a stable nematic phase. Looking at the valleys for S for $\sigma/D = 1.1, 1.2, 1.3$ we found that two nematic regions existed in the simulation with different nematic directors resulting in low values of the global nematic order parameter. In a similar manner for $\sigma/D = 1.4, 1.5$ no global nematic

phase formed for any density. Instead multiple nematic regions appeared with differing nematic directors keeping the global nematic order parameter very small.

However, for $\sigma/D = 1.1, 1.2, 1.3$ a nematic phase begins to form but for the highest packing fractions the nematic order parameter is suppressed again as shown in Fig. 3.7. This suppression happens when global orientational order along a common director reduces, this happens when there is no orientational order or if there are multiple regions with a different director for each region or in a cholesteric phase where the orientation of particles is changing throughout the simulation box. Once a simulation stands out due to a dip or other unexpected behaviour we preform a visual inspection, Fig. 3.8 offers snapshots for $\sigma/D = 1.1, 1.2$, showing regions of local chiral order within the system. However, this is not the cholesteric phase that is commonly thought of and doesn't span the entire system. As with the smaller simulations these local chiral features did not form with expansion from a columnar or smectic phase.

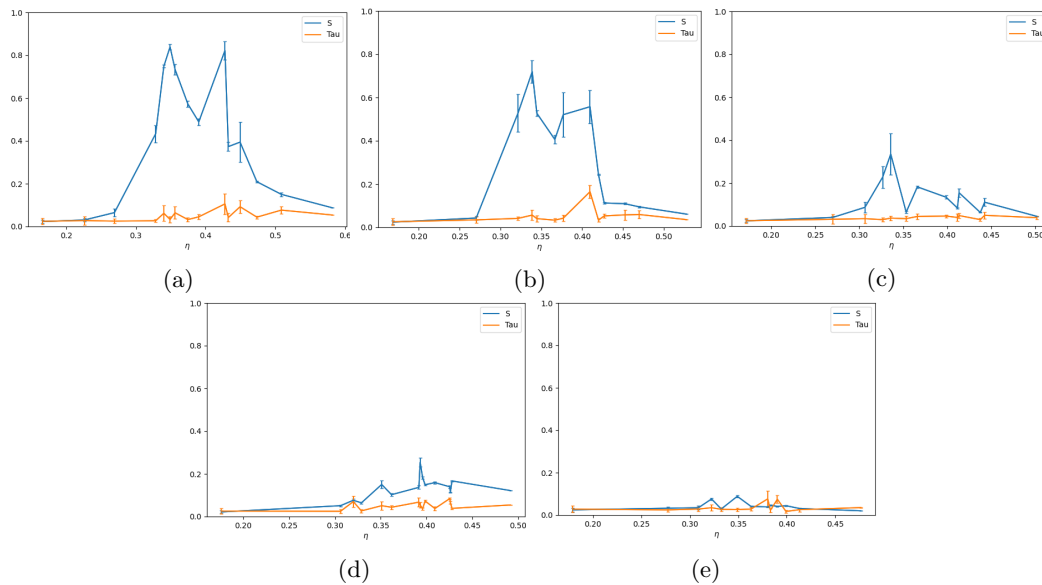


Figure 3.7: Nematic and smectic order parameters plotted against the packing fraction for $\sigma/D = 1.1, 1.2, 1.3, 1.4, 1.5$, respectively. Here we use $L/D = 9$. Points are joined by lines for guidance

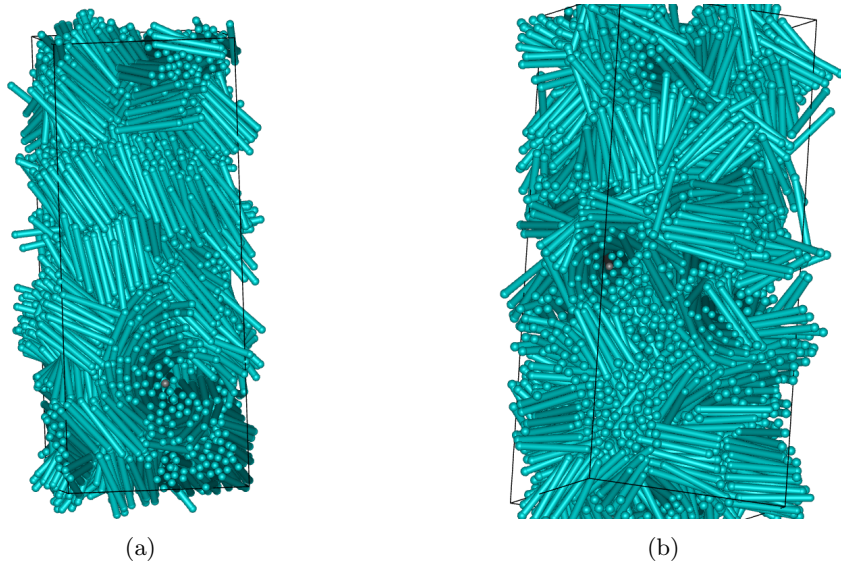


Figure 3.8: Typical configurations of a system of hard dumbbell shaped particles with $L/D = 9$ that were compressed from an isotropic phase. a) shows a double-twisted section in the bottom right, b) again showing a double-twisted section along the edge of the simulation box depicted as a black line.

Extending the length of the particles to $L/D = 13$, the additional stability of the nematic phase that came with extending L has again stabilised the phase and suppressed the chiral order. The smectic phase is not consistently formed by compression from the isotropic phase. The system also fails to form a columnar phase for higher values of σ , because there is not sufficient time for particles to rotate to align to their neighbours. At $\sigma/D = 1.3$ the nematic phase becomes destabilised but from the snapshots it is not clear if chiral features are forming.

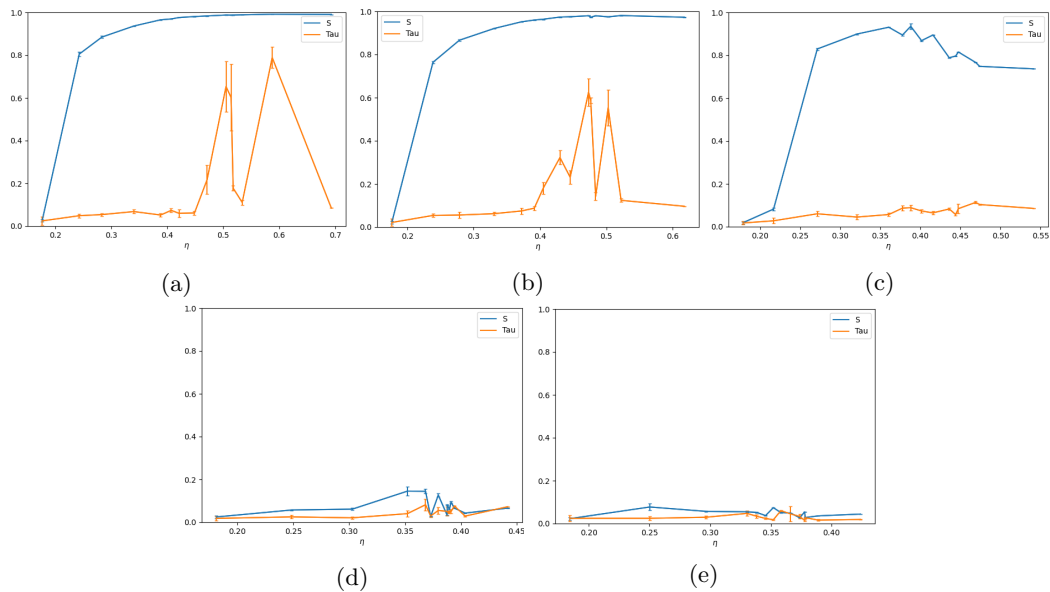


Figure 3.9: Nematic and smectic order parameters plotted against the packing fraction for $\sigma/D = 1.1, 1.2, 1.3, 1.4, 1.5$, respectively. Here we use $L/D = 13$. Points are joined by lines for guidance

3.4 Barbells

In this section the dumbbells are modified by replacing the spheres at the ends with spherocylinders. Previously, we saw that the radius of the capping sphere destabilised the nematic and smectic phases. This time keeping the total length of the particle constant we vary the length of the capping spherocylinders, allowing us to investigate the affect of the length of the convex cavity along the central cylinder. As this length is changed without increasing the radius of the capping shape this may allow us to tune the convex cavity without destabilising the nematic phase in the search for a twisted phase. These simulations were done with the original full periodic boundary conditions. Now σ is the diameter of the spherocylinders on the ends. And L_e is the distance between the hemispheres of the spherocylinders. The volume of these particles is given by

$$V = V_{c1} + 2V_{c2} + 2V_s \quad (3.4)$$

$$V_{c1} = \pi(L - 2(\frac{\sigma}{2} - h))(\frac{D}{2})^2, \quad V_{c2} = \pi(L_e)(\frac{\sigma}{2})^2, \quad V_s = \frac{4}{3}\pi(\frac{\sigma}{2})^3 \quad (3.5)$$

Where V_{c1} is the volume of the centre cylinder, V_{c2} the volume of the other two cylinders, and V_s the total volume of the 2 hemispheres that are part of the spherocylinders.

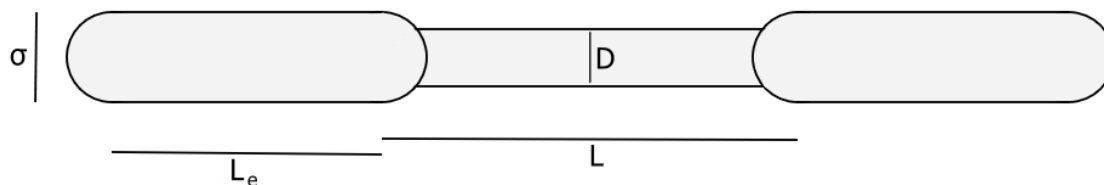


Figure 3.10: Schematic representation of barbell shaped particles.

To investigate the effect of L_e and σ we fix the total length $L + 2L_e = 8$. We skip $\sigma/D = 1$ as it is equivalent to a spherocylinder. With $L_e/D = 0$ we recover a system of dumbbells as considered in the previous sections and in the case of $L_e/D = 4$ spherocylinders are recovered.

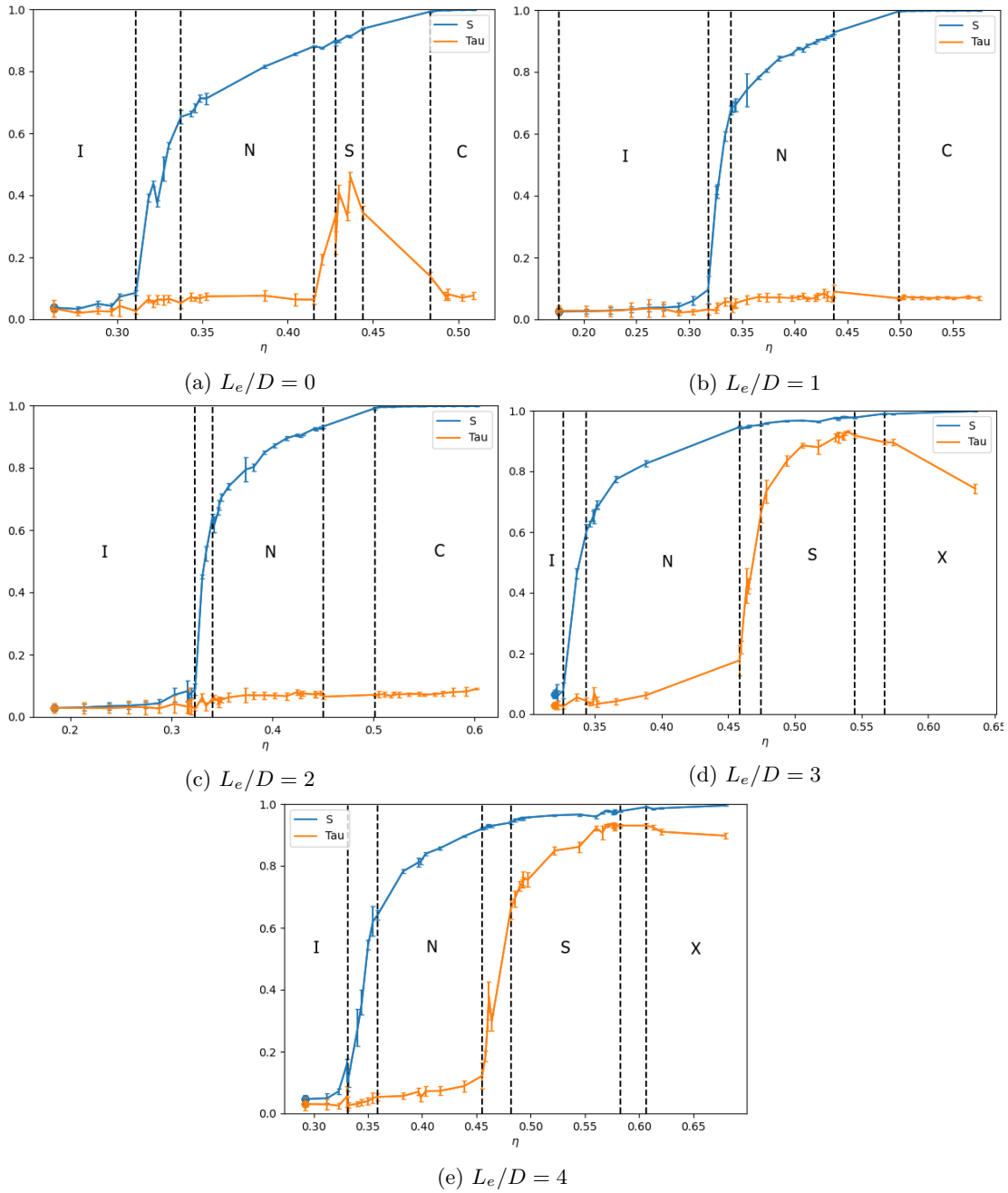


Figure 3.11: Order parameters vs packing fraction for a system of hard barbell shaped particles $L/D = 8.0$, $\sigma = 1.2$. Vertical dashed lines show the phase boundaries between the isotropic(I), nematic(N), smectic(S) and crystal/columnar(X/C) phases.

The different phases of the system are again identified using the nematic and smectic order parameters as well as the packing fraction. The phase transitions are identified in the same manner as in the case of dumbbells. Isotropic-nematic, nematic-smectic, smectic-columnar are shown by the same discontinuities in the order parameters as they were with dumbbells or by a jump in packing fraction for transitions such as the smectic-crystal and nematic-columnar. Snapshots shown in Figs. 3.12 and 3.13 visually confirm that barbells are behaving similarly to dumbbells. Giving additional attention to $L_e/D = 3$ and 4 in Figs. 3.12 & 3.13c the system behaves closer to spherocylinders as the ending spherocylinders from neighbour particles cannot fit into the cavity created by the centre cylinder.

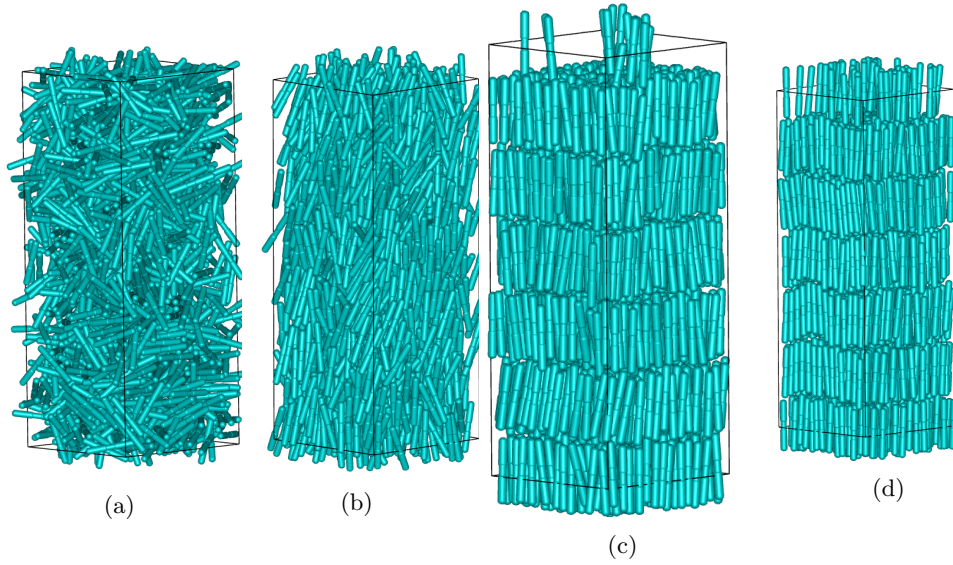


Figure 3.13: a-c) Typical configurations for barbells with $L/D = 8$, $\sigma/D = 1.2$, and $L_e/D = 3$ in the four phases a) isotropic, b) nematic, c) smectic. d) columnar.

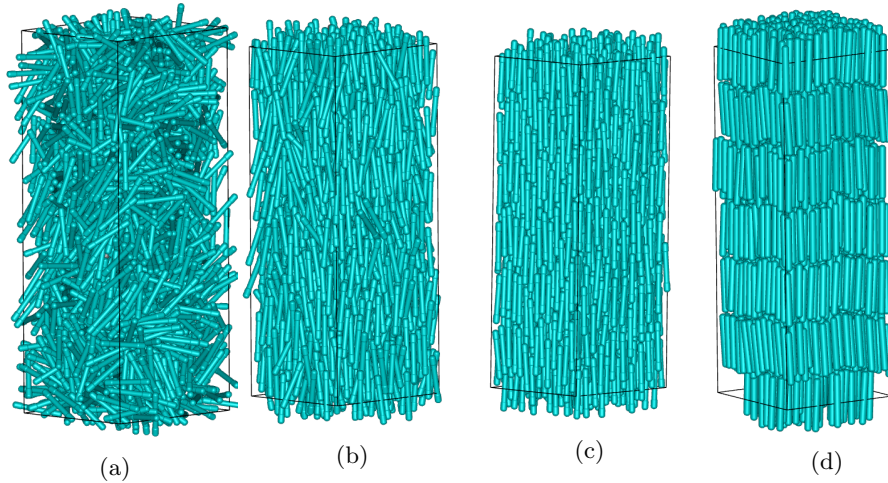


Figure 3.12: a-c) Typical configurations for barbells with $L/D = 8$, $\sigma/D = 1.2$, and $L_e/D = 1$ in the 3 phases a) isotropic, b) nematic, c) smectic. d) When taking $L_e/D = 4$ half the ratio $L/D = 8$, the end spherocylinders overlap with each other leaving a regular spherocylinder.

The phase diagrams in Fig. 3.14 show that the increase of σ/D destabilises the nematic and smectic phases, similar to dumbbells. In Figs. 3.14b and 3.14c the nematic phase gains some stability with increase in L_e/D but the smectic phase is completely absent.

As L_e/D is increased further to three and four, the length of the cylinders on the end is now greater than the length of the concave space created by the central cylinder. The capping spherocylinders can now no longer fit beside the central cylinder and the particles behave more like spherocylinders than barbells. This behaviour gives a stable smectic phase for both $L_e = 3$ and 4. However, $L_e/D = 3$ does not fully stabilise into a crystal phase like a spherocylinders with Fig. 3.11d showing the smectic order parameter falling. There was no appearance of a cholesteric phase or double-twisted columns with barbell shaped particles.

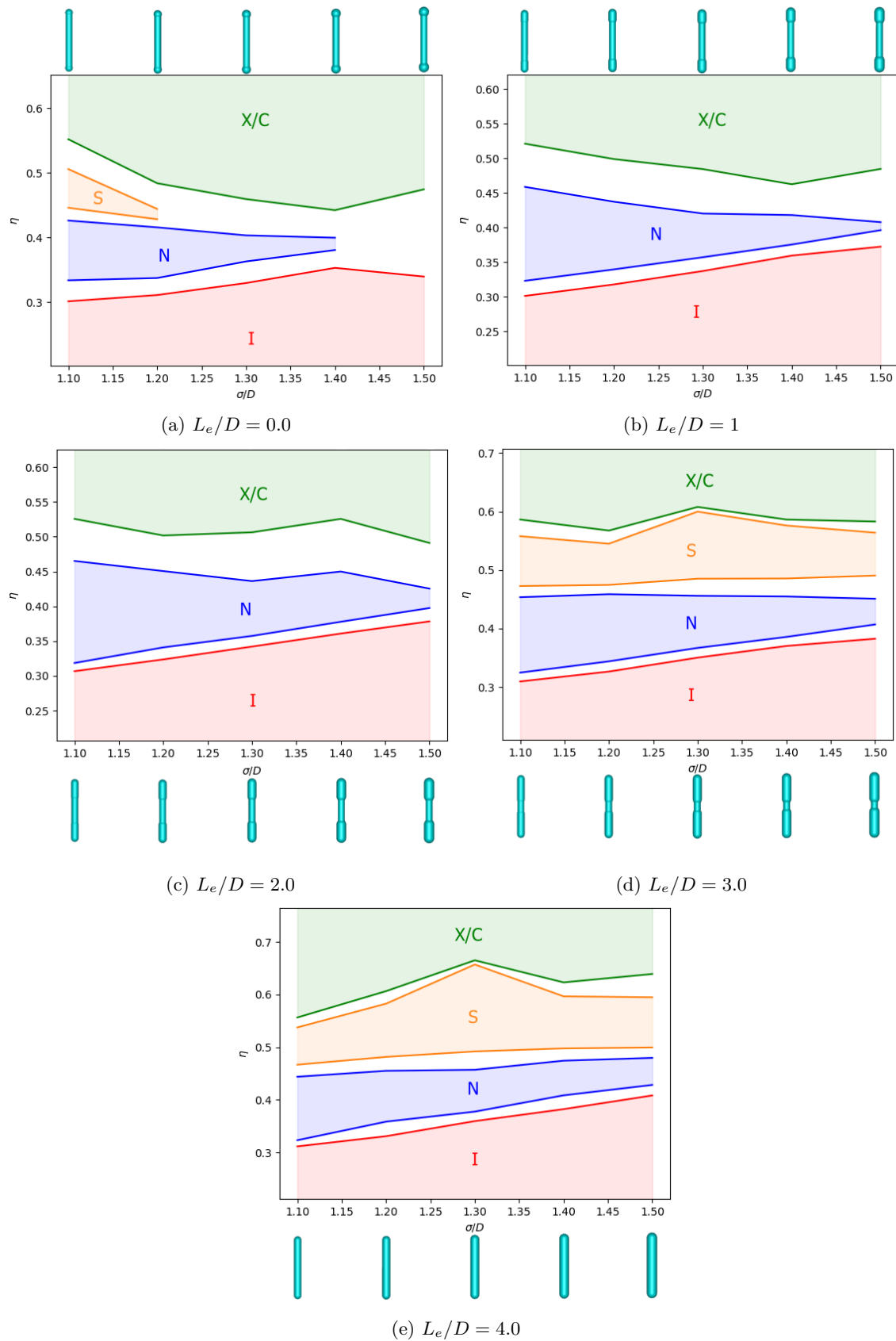


Figure 3.14: Phase diagram of hard barbell shaped particles in the packing fraction η -sphere diameter to rod diameter σ/D representation with a length to diameter ratio of $L/D = 8$ and varying L_e/D . Solid lines denote the phase boundaries of the isotropic (I), nematic (N), smectic (S) and crystal/columnar phase (X/C).

Chapter 4

Conclusion

We investigated the phase behaviour of phase transition for hard dumbbells and hard barbells using Monte Carlo simulations. We gain a performance boost for the simulation using bounding spheres and linked lists to reduce the number of possible overlaps that must be checked.

In this thesis we investigated the effect on the ratio of σ/D on the phase behaviour of dumbbell shaped particles. The results show that increasing this ratio destabilises the nematic phase with respect to the isotropic. Similarly, the crystal phase is destabilised, becoming a columnar phase. This matches the work done by Yang[3] and Gabrielse[4]. We also investigated higher values of $L/D = 13, 15$ and found that the increased length increased the stability of the nematic and smectic phases.

During compression of the system we found the initial configuration impacted phase formation. Compressing the system from a nematic phase reliably formed a smectic phase (for sufficiently small σ/D) or a columnar phase. However, rapidly compressing from an isotropic phase allowed the formation of a racemic of left- and right- handed double-twisted columns. There is no preference for left- or right- handed twisting, which results in the formation of several columns with various handedness and various orientations. With various columns of different handedness the formation of a cholesteric phase, which has a single handedness throughout the simulation box, did not occur and is likely close to impossible to form. These double-twisted features were also suppressed for longer particles $L = 13$ due to the increased stability of the nematic phase.

We also looked at modifying the dumbbells by replacing the sphere on the end with a spherocylinder, referring to them as barbells. For small values of L_e but greater than zero we found the smectic phases was completely destabilised. The nematic phase was still made unstable by the increase in σ/D , but the effect was reduced with the length of the spherocylinders. Once L_e was extended to be sufficiently long that the spherocylinders could not fit into the convex cavity of neighbouring particles, the smectic phase returns as the particles are effectively interacting as spherocylinders. Double-twisted columns were not observed for barbells either.

The formation of double-twisted configurations which exhibit the local twisting predicted by De Gennes was observed but we did not find a true cholesteric phase for either dumbbell or barbell shaped particles. The formation is dependent on the initial configuration, only appearing with compression from the isotropic phase and not appearing with expansion from either smectic or crystal/columnar phases. Thus the double-twisted columns are at best metastable.

Bibliography

- [1] C.-J. Huang, P.-H. Chiu, Y.-H. Wang, & C.-F. Yang *Synthesis of the gold nanodumbbells by electrochemical method*. Journal of Colloid and Interface Science 303, 430–436 (2006).
- [2] B. Peng, *et al.* *Site-specific growth of polymers on silica rods*. Soft Matter 10, 9644–9650 (2014).
- [3] Y. Yang, *et al.* *Liquid-crystalline chiral phase formation and structural transitions of dumbbell-shaped colloids*. <https://www.researchsquare.com/article/rs-50115/v1> (2020) doi:10.21203/rs.3.rs-50115/v1.
- [4] Msc. thesis A.L. Gabrielse Utrecht University *Phase Behavior Of Colloidal ElongatedDumbbells & Lollipops*
- [5] D. R. Link, *et al.* *Spontaneous Formation of Macroscopic Chiral Domains in a Fluid Smectic Phase of Achiral Molecules*. Science 278, 1924–1927 (1997).
- [6] P.G. De Gennes and J. Prost. *The physics of liquid crystals*. No. 83. Oxford university press, 1993.
- [7] C. Vega, & S. Lago, *A fast algorithm to evaluate the shortest distance between rods*. Computers & Chemistry 18, 55–59 (1994).
- [8] T. Van Dijk, *Analysing and improving hash table performance*. 10th Twente Student Conference on IT. University of Twente, Faculty of Electrical Engineering and Computer Science. 2009.
- [9] E. J. Hastings, J. Mesit & R. K. Guha, *Optimization of Large-Scale, Real-Time Simulations by Spatial Hashing*.
- [10] S. Dussi, C. Massimiliano, and M. Dijkstra. *On the stability and finite-size effects of a columnar phase in single-component systems of hard-rod-like particles*. Molecular Physics 116.21-22 (2018): 2792-2805.
- [11] D. A. Walker, E. K. Leitsch, R. J. Nap, I. Szleifer, & B. A. Grzybowski, *Geometric curvature controls the chemical patchiness and self-assembly of nanoparticles*. Nature Nanotech 8, 676–681 (2013).
- [12] B. Birendra *Liquid Crystal - Applications And Uses (Volume 3)*. World Scientific. (1992).

Acknowledgements

I would like to thank my supervisors Prof. Dr. Marjolein Dijkstra and Prof. Dr. René van Roij for all the assistance and guidance offered throughout this master thesis. I would also like to thank Laura Fillion for help with running simulations.